

Spatial Changes of Seasonal Reference Evapotranspiration in Iran Based on CMIP6 Models

Soltani, K.¹  | Masoompour Samakosh, J.¹  | Mojarrad, F.¹  | Hadi Pour, S.²  | Jalilian, A.³ 

1. Department of Geography, Faculty of Literature and Human Sciences, Razi University, Kermanshah, Iran.

2. School of Civil Engineering, Faculty of Engineering, Universiti Teknologi Malaysia (UTM), Johor Bahru, Malaysia.

3. Department of Statistics, Faculty of Science, Razi University, Kermanshah, Iran.

Corresponding Author E-mail: j.masoompour@razi.ac.ir

(Received: 4 Sep 2023, Revised: 21 Sep 2023, Accepted: 26 Sep 2023, Published online: 20 Feb 2024)

Abstract

The aim of the present study is to investigate the spatial changes of seasonal ETo in Iran in the future (2020–2050), based on SSP1-2.6, SSP2-4.5 and SSP5-8.5 scenarios of CMIP6 models (MRI-ESM2 and GFDL-ESM4) compared to the observed data (1992–2014). The FAO56-PM method was used to estimate ETo, and the CV was utilized to investigate the changes. The results showed that ETo will decrease in all seasons across the country under all GFDL-ESM4 scenarios (except winter under SSP5-8.5). However based on the scenarios of the MRI-ESM2 model for 2020–2050, the amount of ETo will increase in the southeastern and southern regions in winter, but in the northwest, west, east, and areas corresponding to the Zagros highlands, ETo will decrease. In spring and summer, ETo will increase in the Caspian Coast, northeastern, western and interior areas of Iran, and even in the northwest (in summer). In the fall, ETo will increase in the eastern and western regions of the country, east of the Caspian Sea and the northern Iranian plateau. Fall, summer, winter and spring, respectively, represent the highest levels of spatial changes in ETo, but it will expand only according to the MRI-ESM2 model in the winter (21% – 25%) under SSP1-2.6. Other seasons show fewer changes than in the past, based on models. Accordingly, the need for detailed planning in water resource management is emphasized, especially in the southern and eastern parts of Iran toward the inner areas.

Keywords: CMIP6, Iran, Seasonal ETo, Spatial Changes.

1. Introduction

Across the world, approximately 66% of the annual precipitation that reaches the surface of the earth is subject to evapotranspiration (Oki & Kanae, 2006); in Iran, this proportion exceeds 70% (Keshavarz et al., 2021). Evapotranspiration is an important process in the energy balance and hydrological cycle, which are related to the carbon cycle (Khanmohammadi et al., 2017; Pan et al., 2020). Evapotranspiration is considered a sensitive indicator of climate and ecosystem feedback (Mokhtar et al., 2020). It is as important as precipitation in atmospheric moisture balance. Estimating evapotranspiration is very important in the calculation of hydrological modeling, water and energy balance, planning water resources, ecosystem health, climate predictions and irrigation planning (Pour et al., 2020a; Shah, 2022). Although temperature and precipitation are

measured at meteorological stations all over the world, other variables are mostly available at only a few stations or have a short data record (Raziei & Perekar, 2021). The time and cost required to directly estimate evapotranspiration increase the need for mathematical models such as Thornthwaite, Penman, Jensen-Haise, Hargreaves-Samani and Penman-Monteith, among other methods (Eslami & Ghahraman, 2013). These methods use two or more climatic variables, such as temperature, radiation, precipitation, relative humidity and wind speed, and various models to estimate the amount of evapotranspiration (Shah, 2022). Therefore, any change in the aforementioned climatic variables would alter the rate of Reference Evapotranspiration (ETo). It is also expected that due to the global warming, which is caused by the excessive emission of greenhouse gases

Cite this article: Soltani, K., Masoompour Samakosh, J., Mojarrad, F., Hadi Pour, S., & Jalilian, A. (2024). Spatial Changes of Seasonal Reference Evapotranspiration in Iran Based on CMIP6 Models. *Journal of the Earth and Space Physics*, 49(4), 175-192. DOI: <http://doi.org/10.22059/jesphys.2023.364373.1007556>

E-mail: (1) kobrasoltani5@gmail.com | f_mojarrad@yahoo.com (2) hpsahar@utm.my (3) jalilian@razi.ac.ir



(GHGs), the ETo of the reference crop and consequently the water needs of plants will be directly affected by climate changes (Heydari & Khoshkhou, 2019).

The emission of GHGs has a significant impact on Earth's climate. Climate scenarios have projected an increase in the world's average temperature for the years 2081–2100 compared to the base period of 1986–2005 (IPCC, 2013). The amount of precipitation and temperature in Iran have changed in the past and will change in future, according to studies that have investigated the long-term trend and changes in various regions of the country (Tabari et al., 2011; Tabari & Talai, 2011; Soltani et al., 2016; Miri et al., 2021), and considering the effect of these variables on evapotranspiration and the relationship of the carbon cycle, energy and water, evapotranspiration is the best indicator of changes in climate and water cycle (Dong et al., 2020).

In recent years, General Circulation Models (GCMs), which represent physical processes in the atmosphere, ocean, cryosphere and Earth's surface, have become the most advanced tools for simulating the response of the global climate system to the increase in GHGs concentration (Majumder, 2015). Currently, Coupled Model Intercomparison Project Phase 6 (CMIP6) models are the latest generation of climate models (CMIP), providing 21 MIPs (Eyring et al., 2016). In the sixth phase, the integration of Shared Socioeconomic Pathways (SSPs) along with Representative Concentration Pathway (RCPs) of GHGs were used to analyze the feedback between climate change and socioeconomic factors such as global population growth, economic development and technological advances. The main quantities include age, gender, education, urbanization and economic development (per capita income). Five main scenarios and a number of sub-scenarios have been designed and used as new scenarios in these models to simulate the future climate (Zarrin & Salehabadi, 2019). The framework of the newly developed scenarios is designed by climate change researchers in such a way that it is able to provide an integrated analysis of future climate impacts, vulnerabilities, adaptation and mitigation. SSP has five narratives of socioeconomic developments, including sustainable development, regional

competition, inequality, development with fossil fuels, and middle development (Riahi et al., 2017). Water resources are highly influenced by climate changes and human activities, especially in semi-arid and arid regions such as Iran, and knowledge of ETo values in these regions plays an important role in water resources management (Sharafi & Mohammadi Ghaleni, 2021).

The results of the studies done in the field of ETo in the past and future periods make it even more clear that it is important to address this issue using the models of the sixth report for Iran. Ajjur and Al-Ghamdi (2021) projected a rise in ETo across the Middle East and North Africa region, up to 0.37 mm/year by the middle of the 21st century (2021–2050) and up to 0.51 mm/year by the end of the 21st century (2071–2100). Liu et al. (2020), in their estimation of evapotranspiration in most regions of the world based on CMIP5 and CMIP6 models, stated that ETo is likely to increase all throughout the 21st century; moreover, this increase based on CMIP6 models will be more than that of CMIP5. Wang et al. (2021) also evaluated 18 CMIP6 models. Although they observed overestimation in most models, they confirmed the increase in ETo during the years 1980 to 2014 in most regions of the world.

Seasonal ETo values based on the Penman-Monteith method in China are also projected to increase using climate models in the years 2020–2099 under RCP scenarios (Zhao et al., 2020), while the case study of Qi et al. (2017) for the years 1964–2013 in the northern regions of China (the largest agricultural region of China) showed a decrease in seasonal ETo except for the winter. The increase in the winter is stated to be a reason for spring draughts. Also, the roles of altitude and latitude are stated to be important factors in the decrease of ETo from the plains to the northern heights of the studied area. A number of national studies in Iran explore the effect of latitude on ETo. For instance, Asadi and Karami (2020) and Shirmohammadi et al. (2018) studied its role in the provinces of Fars and Khorasan Razavi. In addition to latitude, Gudarzi et al. (2018) discussed the role of altitude in ETo decrease in desert areas, Kavir and Makran coasts.

Dong et al. (2020) also examined data from

49 stations (1961–2010) and climate models in Xinjiang, China, and stated that ETo decreased significantly in 1961–1993 and increased again in 1994–2010. But it has been projected to continually increase under the conditions of RCP 4.5 and 8.5. Li et al. (2016) also showed the increase of ETo at a rate of 1.15 mm per year for the period 1991–2013 in the Loess Plateau (China). Obada et al. (2017), in examining the spatial and temporal changes of ETo in West Africa (Benin) in the two periods of 1981–2010 and 2011–2100 using the PM method, concluded that the amount of ETo has alternately increased and decreased in the past, but the annual and seasonal scales will gradually increase in the future.

Some studies conducted in Iran also show an increase in the values of this variable during the past and future periods. Alizadeh and Salehnia (2014), using the PM method, demonstrated the maximum increase in ETo in the south and southwest of Iran, its annual increase in the northeast, and an overall increase in ETo during the statistical period by examining data from 50 years (1961–2010) at 30 synoptic stations from different climates of Iran. The study of Masoompour et al. (2014) indicates an increase in ETo during the statistical period of 1981–2009 in Iran, especially in the southeast, center and southwest, and the lowest amount was observed in the north of the country. The study by Nouri et al. (2017), using data from scenario B2 of the HadCM3 model, showed an increasing trend of ETo in the current century for the stations under study in the northwest and west of Iran. The largest increase was estimated to last until 2040 for the spring and until 2100 for the fall. Cheshmberah and Zolfaghari (2019) projected the increase of ETo in the northwest, west, center and south of Iran during the years 2020–2049 using the Penman Monteith of FAO56 (FAO56-PM) method, NCEP network data, and the Had-cm3 model. Kadkhodazadeh et al. (2022) also estimated an increase in ETo under both pessimistic and optimistic scenarios for the period of 2021–2050 at stations in the northwest using CMIP6 models. Iraq, as one of the countries contiguous with Iran and sharing the same latitude, has had a significant increase in ETo during the last four decades (1981–2021), especially in

summer (Al-Hasani & Shahid, 2022). The only available study for Iran in the sources for ETo projection using CMIP6 models is the Modaresi and Araghi study (2023). Using an artificial neural network, they showed that ETo will increase in 2031–2060 and 2061–2090 under SSP1-2.6 and SSP5-8.5 scenarios.

The primary goal of this research is to analyze seasonal ETo changes in Iran from 2020 to 2050 using the SSP1-2.6, SSP2-4.5 and SSP5-8.5 scenarios from the CMIP6 series of oceanic-atmospheric models and compare the future to the years 1992–2014. The findings of this study can demonstrate how possible future changes can affect ETo and be used in climate planning.

2. Methods

2-1. The study area

Iran (Figure 1) is located in the southwest of Asia, and the Oman Sea and the Persian Gulf in the south and the Caspian Sea in the north form part of its borders. Iran is located on the northern margin of the subtropical high-pressure system. Iran is a mountainous country with mountain ranges such as Alborz and Zagros, which separate the inner regions of Iran from the marginal regions of the north and south of the country. The eastern part of the plateau is covered by two salt plains, Kavir and Lut. Iran has two lowlands in the southwest (Khuzestan) and the north (coast of the Caspian Sea) (Rahimi, 2012; Lashkari & Mohammadi, 2019; Maghsoudi, 2020).

Annual precipitation and average daily temperature are directly related to the topography and latitude of the country. The amount of precipitation gradually decreases from the northwest to the southeast. However the average daily temperature follows the opposite pattern of precipitation and gradually increases from the northwest to the southeast of Iran. The average daily temperature is lower along the Zagros mountain range in the west and the northwestern highlands but higher in the southern coastal areas. Potential evapotranspiration in Iran does not follow the geographical distribution of temperature and its highest rate is observed in the southwest and southeast of the country, while the lowest rate is observed in the northwest corner of the country. In the central region,

evapotranspiration has a middle value and gradually decreases toward the south and north of the country. High potential evapotranspiration and less precipitation have made the climate of the country mostly arid and semi-arid (Pour et al., 2020b).

2-2. Data

The data (Table 1) was provided by the Islamic Republic of Iran Meteorological Organization (IRIMO) for a 23-year period (1992–2014) for 102 synoptic stations (Figure 1). Due to a defect in the sunshine duration data, values from 1992 onwards were used. Run test was used to check the quality of the data.

The model data (Table 1), including the MRI-ESM2-0 and GFDL-ESM4 models for the years 2020–2050 were obtained according to the GCMeval classification under the SSP1-2.6, SSP2-4.5, and SSP5-8.5 scenarios, with a spatial resolution of 100 km. Afterwards, using the "Resampling Technique", the bilinear method within the

raster R package (Hijmans et al., 2015), it was converted to data with a resolution of 50 km. This method performs a bilinear interpolation and determines the new value of a cell based on a weighted distance average of the four nearest input cell centers. It is useful for continuous data and will cause some smoothing of the data (Amare et al., 2021). The output cell size parameter can resample the output to the same cell size as an existing raster layer, or it can output a specific X and Y cell size. The cell size can be changed, but the extent of the raster dataset will remain the same. After that, calculations were done using equations 1 to 3. Next, the maps were drawn in the Lambert system. Due to the lack of data on sunshine hours in the CMIP6 models, this variable was calculated using surface downwelling (longwave and shortwave) radiation and surface upwelling (longwave and shortwave) radiation data (Table 1) from the models and the radiation estimation method of Li et al. (2019).

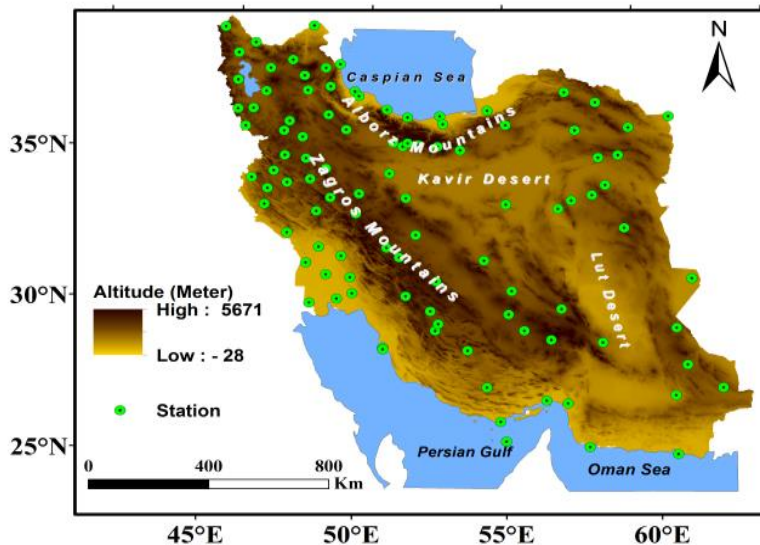


Figure 1. The location of the studied synoptic stations.

Table 1. Characteristics of the Data used in the Study.

Data center	Data	Characteristic	Statistical period
Iran Meteorological Organization (IRIMO)	Maximum and minimum temperature at 2 m of height; wind speed at 2 m of height; sunshine duration for 102 synoptic stations.	Monthly	1992- 2014
Earth System Grid Federation (ESGF)	Surface Downwelling Longwave Radiation (rlds); Surface Downwelling Shortwave Radiation (rsds); Surface Upwelling Longwave Radiation (rlus); Surface Upwelling Shortwave Radiation (rsus); Maximum and minimum temperature at 2 m of height; wind speed at 2 m of height.	Monthly GFDL-ESM4 MRI-ESM2-0 Spatial resolution of 100 Km	2020- 2050

2-3. Methods

2-3-1. GCMeval

GCMeval is a tool for selecting and evaluating global climate models. This tool was created using the "Shiny" package in R software (Chang et al., 2017) and is also available to users as an online program through <https://gcmeval.met.no/>. By evaluating climate models from the CMIP5 and CMIP6 ensembles and a subset of models, GCMeval discards the worst-performing climate models and attempts to retain the full ensemble of models with the best statistical performance. One of the advantages of this tool is the determination of "weights for skill evaluation", including the importance of the study area, variables, seasons and evaluation scores (such as bias, spatial correlation and RMSE). Based on these choices, the climate models are ranked according to the representation of the past climate. Under "Advanced Settings," the reference data set that the GCM simulations are measured against can be changed. Plots of the predicted mean change in temperature and precipitation in the target region for the past (1981–2010), the near future (2021–2050), and the far future (2071–2100) are also included in GCMeval. The Global Precipitation Climatology Project (GPCP) data set, along with temperature and precipitation data from two global reanalyses of the European Centre for Medium-Range Weather Forecasts, ERA5 and ERA-Interim, are currently used to calculate evaluation statistics (Parding et al., 2020). In this study, the tool was used to select the models, but due to the lack of some required variables, the fourth- and fifth-rank models were taken (Figure 2). Figure 2 shows the annual mean

temperature and precipitation change within the study area from the past (1981–2010) to the near future (2021–2050) based on the ERA5 and GPCP data sets, respectively.

2-3-2. Calculation of PM-FAO56

Although calibrated methods such as Hargreaves-Samani (Newton et al., 2021) and Blaney-Criddle (Heydari et al., 2015) have also shown good results, the FAO56-PM method has been proposed as the standard method for calculating reference ETo by Allen et al. (1998), the International Committee on Irrigation and Drainage (ICID), and the World Meteorological Organization (WMO) (Kermani et al., 2014). In the present study, evapotranspiration was estimated using the method defined in the Standardized Precipitation-Evaporation and Transpiration Index Package (SPEI Package) (Begueria et al., 2017). This method uses the main parameters introduced by Allen et al. (1994) to calculate ETo based on the FAO56-PM method as follows (Bakhtiari et al., 2017):

$$ET_o = \frac{0.408\Delta(Rn-G) + \gamma \left[\frac{900}{T+273} \right] u_2 (e_s - e_a)}{\Delta + \gamma(1+0.34u_2)} \quad (1)$$

where ETo is the reference evapotranspiration (mm day^{-1}), Rn is the net solar radiation ($\text{MJ m}^{-2} \text{day}^{-1}$), G is the soil heat flux density (mm day^{-1}), T mean is the maximum and minimum daily temperatures at two meters of height ($^{\circ}\text{C}$), u_2 is the wind speed measured at two meters of height (m s^{-1}), e_s is the saturation vapor pressure (k Pa), e_a is the actual vapor pressure (k Pa), $(e_s - e_a)$ is the saturation vapor pressure deficit (k Pa), Δ is the slope of saturation vapor pressure curve ($\text{mb } ^{\circ}\text{C}^{-1}$) and γ is the psychrometric constant ($\text{kPa } ^{\circ}\text{C}^{-1}$).

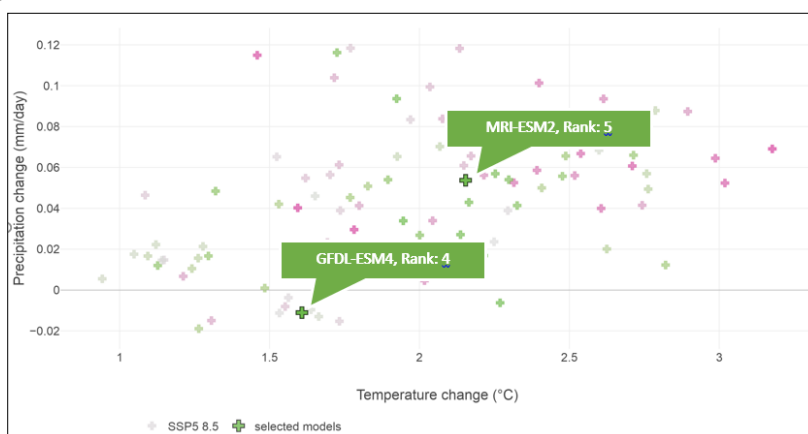


Figure 2. The figure includes GCM runs for emission scenario SSP5-8.5 (purple) and selected models (green) from the CMIP6 ensemble in focus region (in this study, West of Asia [WAS: 19]).

Since solar radiation data is rarely available, the code in the SPEI package estimates it through sunshine duration or cloud cover percentage. In the absence of pressure data, calculations can be done using dew point temperature, relative humidity, or minimum temperature. The surface pressure required to calculate the humidity is also calculated through the atmospheric pressure at sea level and the height of the points above sea level; otherwise, it is considered to be 101.3 kPa (Begueria et al., 2017).

2-3-3. Coefficient of variation (CV)

After calculating the seasonal mean values, standard deviation, and finally Coefficient of Variation (CV) for ETo were calculated seasonally as follows (Mulla & McBratney, 2001):

$$SD = \sqrt{\frac{\sum(x_i - \bar{x})^2}{N}} \tag{2}$$

$$CV = \frac{SD}{\bar{x}} \times 100 \tag{3}$$

In the above equations, X_i is the average of each season of the year, \bar{X} is the total average and N is the number of years. CV is calculated by dividing the standard deviation by the mean. In the above equation, SD is the standard deviation and \bar{X} is the total mean. Its result is multiplied by 100 to be expressed as a percentage.

3. Results and discussion

3-1. Spatial distribution of ETo in 1992–2014

Figure 3 depicts the spatial distribution of the seasonal mean ETo in winter (January–February–March), spring (April–May–June), summer (July–August–September), and fall

(October–November–December), with summer (Figure 3c) having the most ETo during the statistical period. Southwest Iran has had the highest values this season, with 0.5% of the area (Table 2). Next, southwest stations, eastern and southeastern regions had the highest levels of ETo in spring (Figure 3b), fall (Figure 3d) and winter (Figure 3a). Regions in the northern half of the country, however, have the lowest levels of ETo, especially the Caspian coast and the northwestern part of the country, including the northern coast of the Oman Sea in the summer. Across the region, higher latitudes and altitudes have a significant decreasing effect on ETo. That is, the amount of ETo decreased from lower latitudes to higher latitudes and from plain areas (low altitude) to mountainous regions (high altitude) as reported by Asadi and Karami (2020), Gudarzi et al. (2018) and Shirmohammadi et al. (2018) in several study regions of Iran, as well as Qi et al. (2017) in China. This was demonstrated by the behavioral consistency of ETo with regard to the latitude and mountainous regions in the displayed spatial patterns during the study period (past and future).

In all seasons of the year during the observational period, except for summer, when some areas of the southeast, especially the coastal areas, have a decrease in ETo under the influence of the monsoon system, higher values of ETo are included in the southwest, southeast, and south of the country towards the interior areas, which confirms the findings by Masoompour et al. (2014).

Table 2. Average seasonal ETo percentage and area, 1992–2014.

Season	Value (mm)	Area (Km ²)	Percentage
Winter	90 - 230	682691.1	42
	230.1 - 380	880724.6	54.2
	380.1 - 522	61434.8	3.8
Spring	285 - 605	645217.1	39.7
	605.1 - 920	955283.9	58.8
	920.1 - 1240	24349.5	1.5
Summer	360 - 775	780865.9	48.1
	775 - 1180	834745.6	51.4
	1180.1- 1690	9239	0.5
Fall	140 - 320	892553.9	54.9
	320.1 - 505	724266.4	44.6
	505.1 - 690	8030.2	0.5
Sum		1624850.5	100

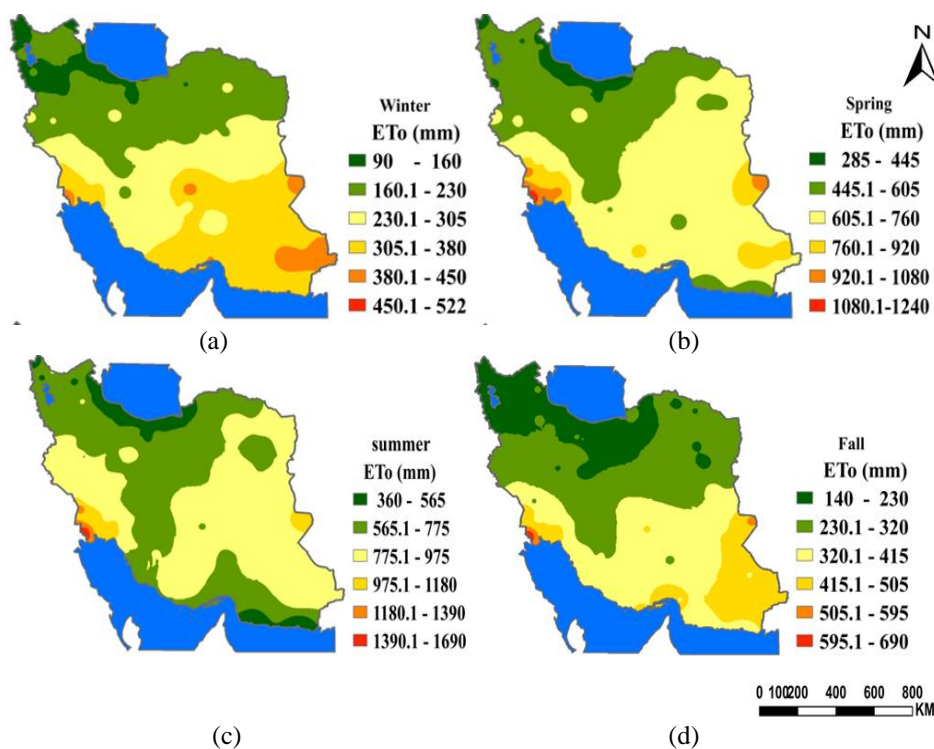


Figure 3. Average seasonal ETo for 1992–2014. (a) Winter, (b) Spring, (c) Summer, (d) Fall.

3-2. Spatial distribution of ETo in 2020–2050

The output maps of the average winter ETo in 2020–2050 in Figure 4a to 4f show that under the conditions of SSP5-8.5 of the GFDL-ESM4 model, ETo will increase and based on the other two scenarios, decrease, especially in the northern half of Iran.

However, based on all the MRI-ESM2 scenarios, regions in the southeast, to some extent, the east towards the interior regions of Iran will witness a rise in evapotranspiration. These areas, as well as regions in the northern half with less ETo will expand (Table 3).

Table 3. Average seasonal ETo percentage and area, 2020–2050.

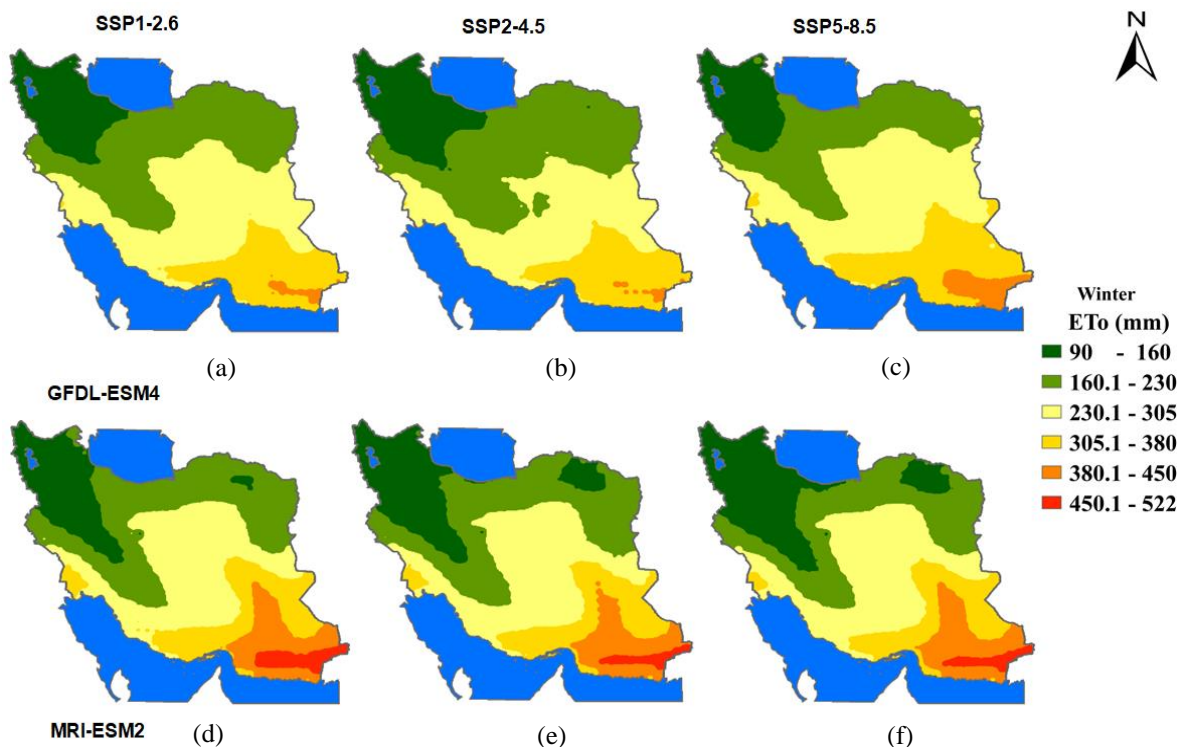
Season	Scenario Model	SSP1-2.6		SSP2-4.5		SSP5-8.5	
		Area (Km ²)	Percentage (%)	Area (Km ²)	Percentage (%)	Area (Km ²)	Percentage (%)
Winter	GFDL-ESM4	782118	48.1	880724.6	54.2	651261.3	40.1
		824988.5	50.8	732771.5	45.1	910038.9	56
		17744	1.1	11354.4	0.7	63550.3	3.9
	MRI-ESM2	728540.5	44.8	762085.8	46.9	757034.6	46.6
		705918.1	43.5	696161	42.8	689512.3	42.4
		190391.9	11.7	166603.7	10.3	178303.6	11
Spring	GFDL-ESM4	1077290.2	66.3	1083377.6	66.7	1050436.7	64.6
		547560.3	33.7	541472.9	33.3	574413.8	35.4
		0	0	0	0	0	0
	MRI-ESM2	383158.4	23.6	391274.8	24.1	406903.4	25
		956276.9	58.8	956967.7	58.9	939482.7	57.8
		285415.2	17.6	276608	17	278464.4	17.2
Summer	GFDL-ESM4	817217.4	50.3	811389.1	49.9	779398.1	48
		807633.1	49.7	813461.4	50.1	845452.4	52
		0	0	0	0	0	0
	MRI-ESM2	103010.2	6.3	103442	6.4	101024.3	6.2
		1316597	81	1325274.6	81.6	1272776.5	78.3
		205243.3	12.7	196133.9	12	251049.7	15.5
Fall	GFDL-ESM4	1042795.2	64.2	1040766	64.1	978985.8	60.3
		582055.3	35.8	584084.5	35.9	645864.7	39.7
		0	0	0	0	0	0
	MRI-ESM2	686403.9	42.2	674574.6	41.5	639431.9	39.4
		788032.6	48.5	815188.3	50.2	832198.4	51.2
		150414	9.3	135087.6	8.3	153220.2	9.4
Sum		1624850.5	100	1624850.5	100	1624850.5	100

The pattern of projected outcomes of scenarios in spring (Figure 4) and the scope of the regions (Table 3) show the reduction of ETo in most regions of Iran except the eastern half of the Caspian coast and the coast of Oman, based on all GFDL-ESM4 scenarios (Figure 4m, n and o). However, based on the MRI-ESM2 scenarios (Figure 4p, q and r), an increase in the extent of the highest ETo values in the southeast, east and south of Iran towards the inner regions is projected compared to the observational period. Based on the scenarios of this model, the extent of the areas with less ETo in the northeast of the country, the eastern areas of the southern shores of the Caspian Sea, and the west of the country has been reduced and replaced by areas with medium ETo (Figure 4 and Table 3).

According to Table 3, GFDL-ESM4 shows a drop in the extent of areas with low summer ETo values (increasing ETo) on the southern coasts and shows an increase in the northeast and west of Iran under the conditions of SSP1-2.6, SSP2-4.5 and SSP5-8.5 scenarios (Figure 5a, b and c). Areas with more ETo in the southwest will be removed and replaced by areas with medium ETo under the conditions of SSP1-2.6, SSP2-4.5 and SSP5-8.5 scenarios (Figure 5a, b and c). However the spatial distribution of ETo based on MRI-ESM2 scenarios (Figure 5d, e and f) shows a

severe decline in areas with low levels of ETo and an increase in areas with medium ETo (in the northeast, to some extent the east, the west, parts of the northwest, interior areas, and the southern coasts of Iran) and the most (in the southwest, southeast and east of the country) for the summer of 2020 to 2050 (Table 3).

GFDL-ESM4 fall seasonal average distribution of ETo (Figure 5m, n and o) shows that the amount of ETo in Khuzestan will decrease to the lowest values (230.1-320 mm) in the period of 2020 to 2050 compared to the observational period (505.1-690 mm), which was the most amount of ETo in Iran. Also, the amount of ETo in the southeast and southern coasts of the country is estimated to decline based on the scenarios of this model. However, according to MRI-ESM2, the extent of the areas with less ETo in the northeast and the interior areas of Alborz and Zagros towards the central plateau of Iran has decreased compared to the observational period, and the extent of the areas with medium ETo (in the southeast, east and south towards the interior areas) will increase under all three scenarios. The same change will happen to areas with the most amount of ETo (in the southeast of the country and the coasts of Oman) (Figure 5p, q and r and Table 3), especially under SSP5-8.5 (Figure 5r).



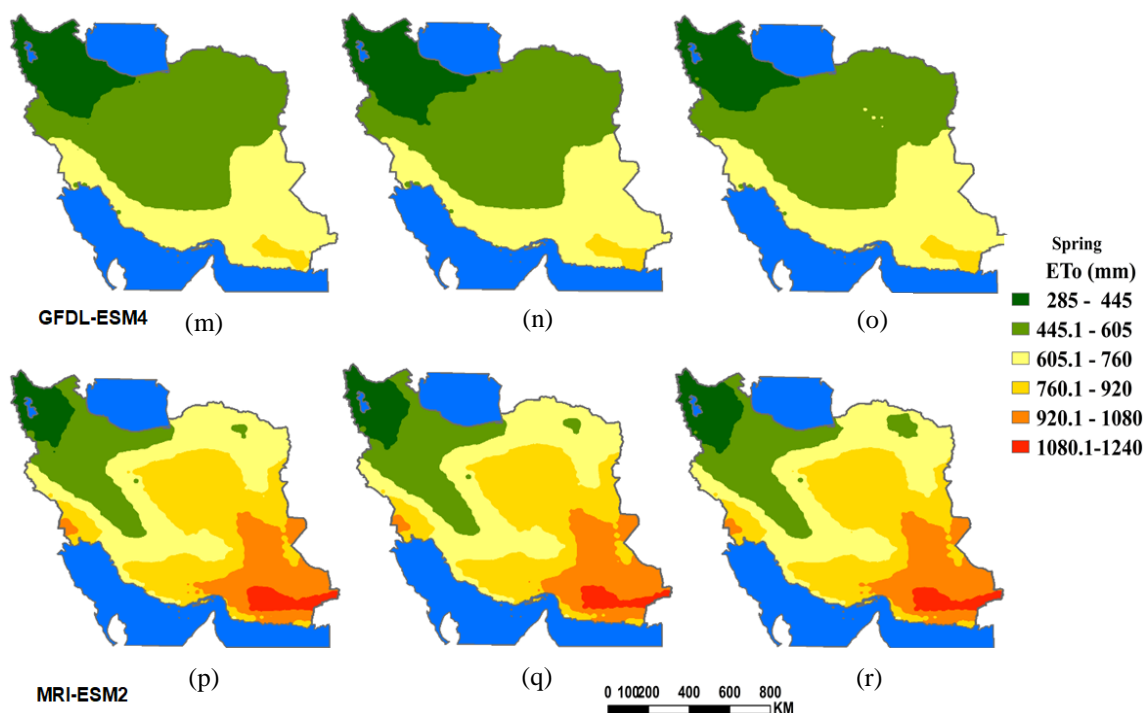


Figure 4. Average seasonal ETo, in Winter (a to f) and Spring (m to r) under scenarios SSP1-2.6, SSP2-4.5 and SSP5-8.5 for 2020–2050.

The findings of Nouri et al. (2017), demonstrating an increasing trend of ETo in the northwest and west of Iran in the spring of 2011 to 2040, is not confirmed based on the data period in this study (2020–2050). This may be because of the difference in the length of periods under investigation by the two studies, as well as improvements in the sixth report compared to the fourth report. Additionally, rather than using the historical data from the models, the present study compares the possibilities for the future to the observational data. The findings of Kadkhodazadeh et al. (2022) regarding the rise of ETo in the same statistical period under optimistic and pessimistic scenarios in northwest Iran based on Figures 2 to 4 in the present study were observed only in the average summer of the MRI-ESM2 model.

In general, the present study confirms the findings of Modaresi and Araghi (2023) regarding the increase of ETo in the periods of 2031–2060 under the SSP1-2.6 and SSP5-8.5 scenarios and its greater increase in arid environments, the findings of Liu et al. (2020) regarding the global increase of ETo, the findings of Ajjur and Al-Ghamdi (2021) proving the rise of ETo in the Middle East and North Africa, and the findings of Zhao et al. (2020) in China, under all MRI-ESM2 scenarios for all seasons, as well as SSP5-8.5

from the GFDL-ESM4 model in the winter, except for the northwestern areas and some areas in Zagros and the western half of the Caspian coast (except for the summer, when the MRI-ESM2 model predicts an increase in these areas as well). These findings are confirmed by both models in comparison to the national average.

3-3. Spatial changes in ETo from 1992 to 2014

The CV of winter ETo in Iran (Figure 6a) shows that the most changes (21% - 25%) occurred in 0.9% of the country's regions, which are scattered in the northwest, northeast and southeast of the Caspian Sea, as well as the southeast of the central plateau. Besides, the lowest CV (4% - 8%) occurred in 0.9% area on the southern coast of the country. Spring (Figure 6b) witnessed a decrease in changes compared to winter, but the most CV (18% - 21%) is associated with the same regions, with the core in the southeast of the Central Plateau (Kerman) in 0.2% of Iran. The lowest CV (4% - 7%) was found in 11.2% of the country, from the south coast to the interior regions.

In summer (Figure 6c), the changes around Kerman (0.2% of the country) have increased to 23% - 28%, and except for the southeast of the Caspian coast, the changes have been up

to 12% in almost all other regions of the country. The lowest CV (2% - 7%) has occurred in the northwest towards the western part, southern coasts and interior areas in 34.3% of Iran.

In fall (Figure 6d), CV has increased in the interior and northern half of the country, and

the most spatial changes (27% - 32%) occurred around Kerman and the southeast of the Caspian Sea (in 0.4% of the area). The lowest changes of this season (5% - 10%) have been in the south of the country, especially the coasts (in 11% of the area).

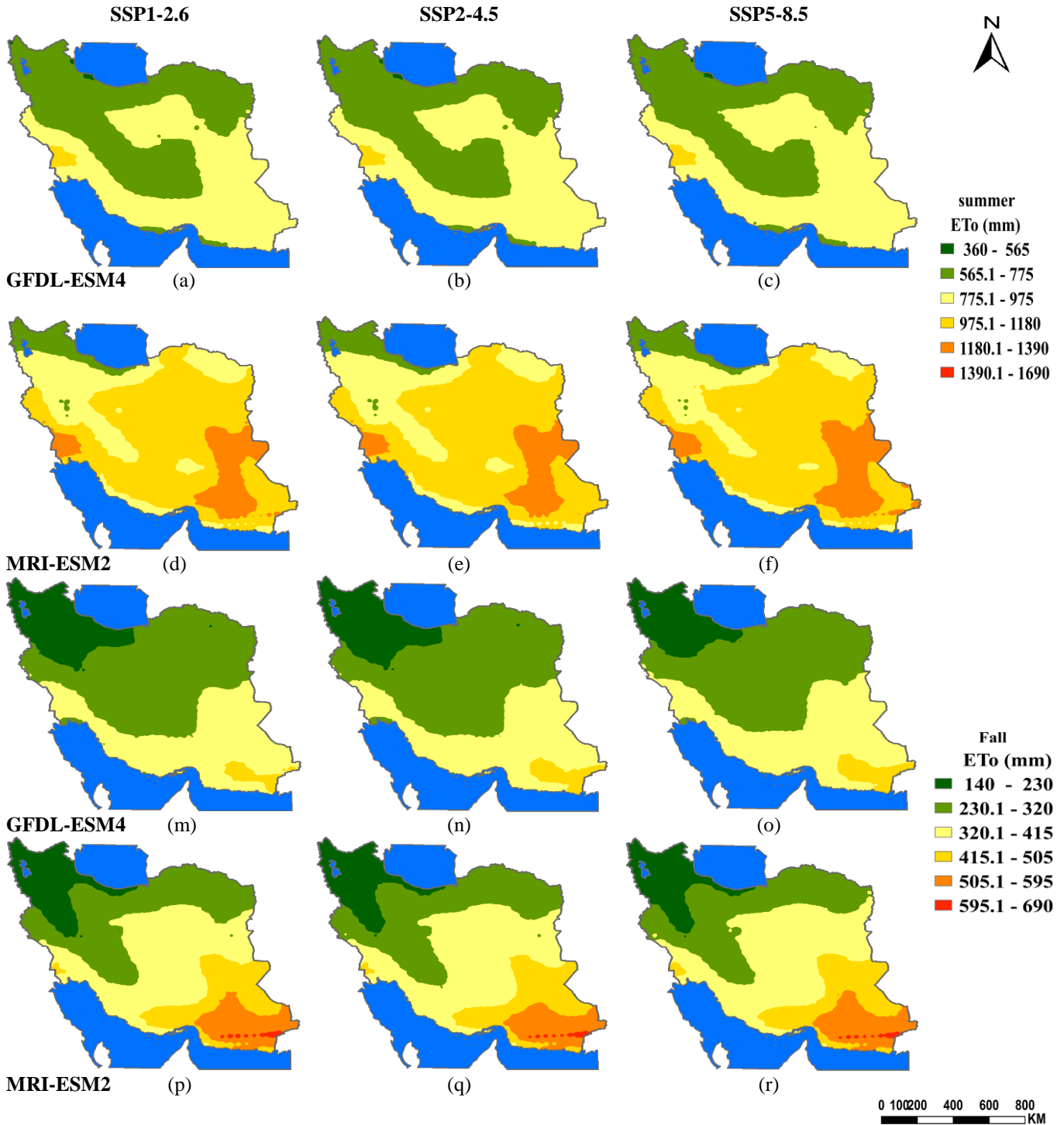


Figure 5. Average seasonal ETo, in Summer (a to d) and Fall (m to r) under scenarios SSP1-2.6, SSP2-4.5 and SSP5-8.5 for 2020–2050.

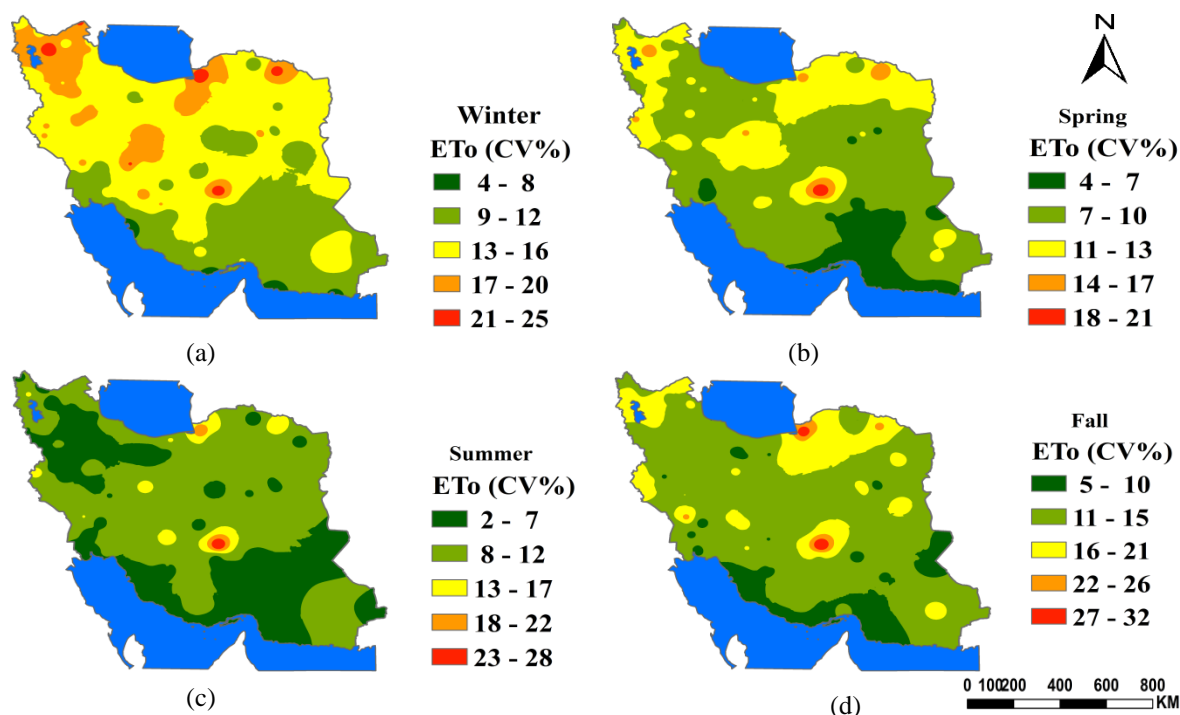


Figure 6. Average seasonal ETo changes for 1992–2014. (a) Winter, (b) Spring, (c) Summer, (d) Fall.

3-4. Spatial changes in ETo from 2020 to 2050

The projection of GFDL-ESM4 scenarios for the winter of 2020–2050 show that under scenarios 1-2.6, 2-4.5 (Figure 7a and b) the extent of areas with low changes (4% - 8%) in south coasts and northwest and under SSP5-8.5 (Figure 7c), in the western and interior regions of the country will increase from 0.9% (observational) to 14.8%, 17.5% and 55.6%, respectively. Most of changes also decrease in the northern half and the internal plateau. However, according to MRI-ESM2, in the conditions of the SSP1-2.6 scenario (Figure 7d), the changes will increase in other regions of Iran, except for some areas in the northwest, and the vastness of areas with most of the changes reaches 16% compared to the observational period (0.9%). In the conditions of SSP2-4.5 (Figure 7e), the areas with the least and most changes will be removed, and the areas with medium changes (13% - 16%) will be increased. In the conditions of SSP5-8.5 (Figure 7f), the extent of the areas with medium changes will increase from 13% to 46.2%, except for the northwest towards the west of the country.

Based on the patterns of GFDL-ESM4 scenarios, the amount of changes in ETo for the spring of 2020–2050 will decline from 11%–17% in the northern half and the inner regions of the Iranian plateau to 4%–10%.

Moreover, the area that it affects will increase from 11.2% in the observational period to 78.4%, 66.4% and 62.3% under scenarios SSP1-2.6, SSP2-4.5 and SSP5-8.5, respectively (Figure 7m, n and o). According to the MRI-ESM2 scenarios (Figure 7-p, q and r), in spring, the changes in the southeast of the Caspian Sea and the interior areas will decrease to 4%–10% compared to the base period 14%–21%), but will increase in the conditions of SSP2-4.5 and SSP5-8.5 (Figure 7q and r) in the northwest and South Zagros. In general, based on all three scenarios of this model, the extent of the areas with the low change in the southern half of Iran and the east will increase from 11.2% to 26.6%, 34.6% and 36.1%, respectively, in the SSP1-2.6, SSP2-4.5 and SSP5-8.5 scenarios.

The results showed that based on GFDL-ESM4 and MRI-ESM2, the average of changes in summer ETo will decrease to 2%–12% for the statistical period of 2020 to 2050 (Figure 8a to d), and only will be 13%–17% in the northwest corner of Iran under SSP2-4.5 and SSP5-8.5 of MRI-ESM2 model (Figure 8e and f).

Based on all GFDL-ESM4 and MRI-ESM2 scenarios in fall (Figure 8m to p), in addition to a decrease in changes in the southeast of the Caspian Sea and around Kerman from 27%–32% to 5%–15%, the changes in other regions of Iran will also decrease.

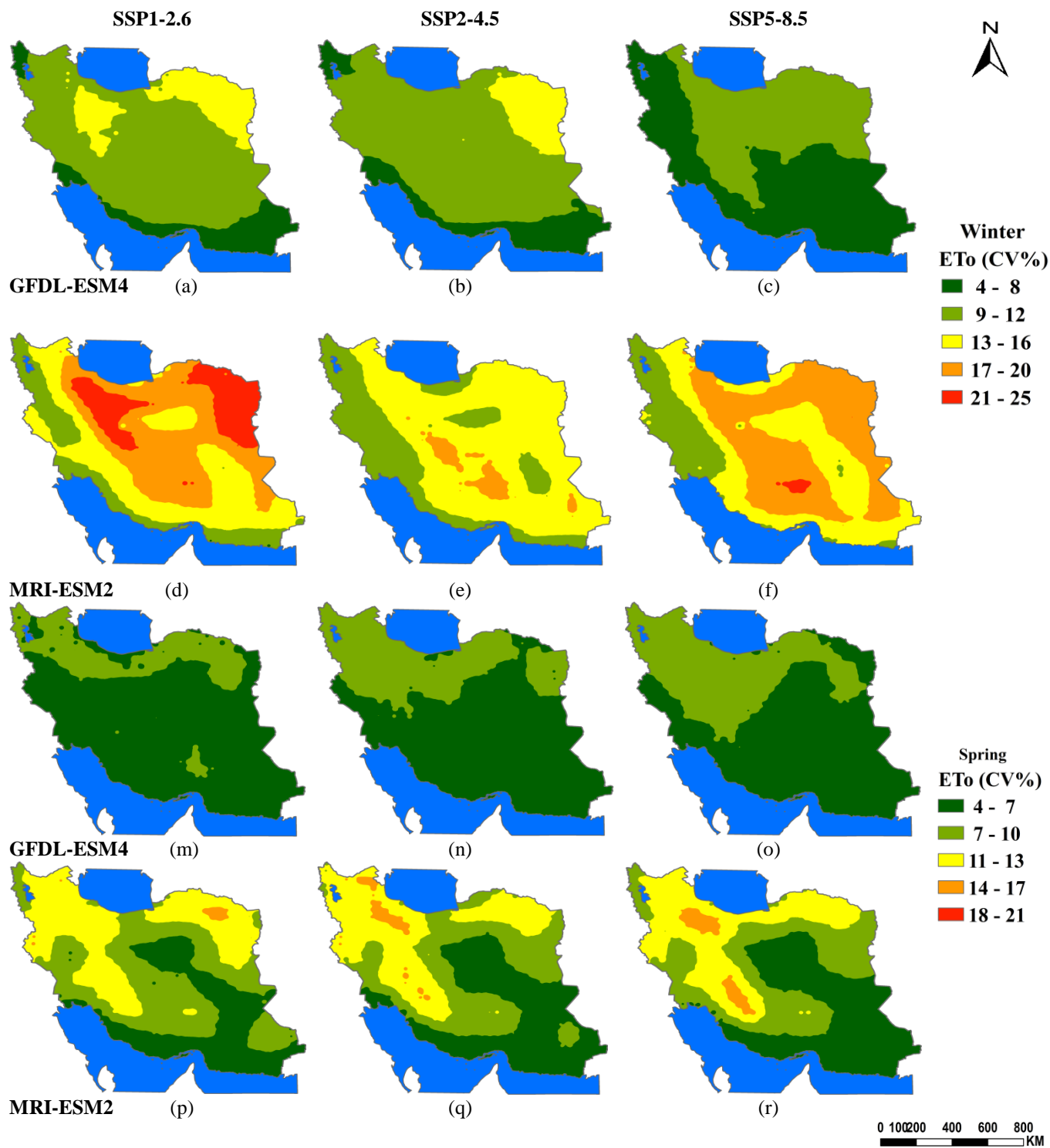


Figure 7. Average seasonal ETo changes in Winter (a to f) and Spring (m to r) under scenarios SSP1-2.6, SSP2-4.5 and SSP5-8.5 for 2020–2050.

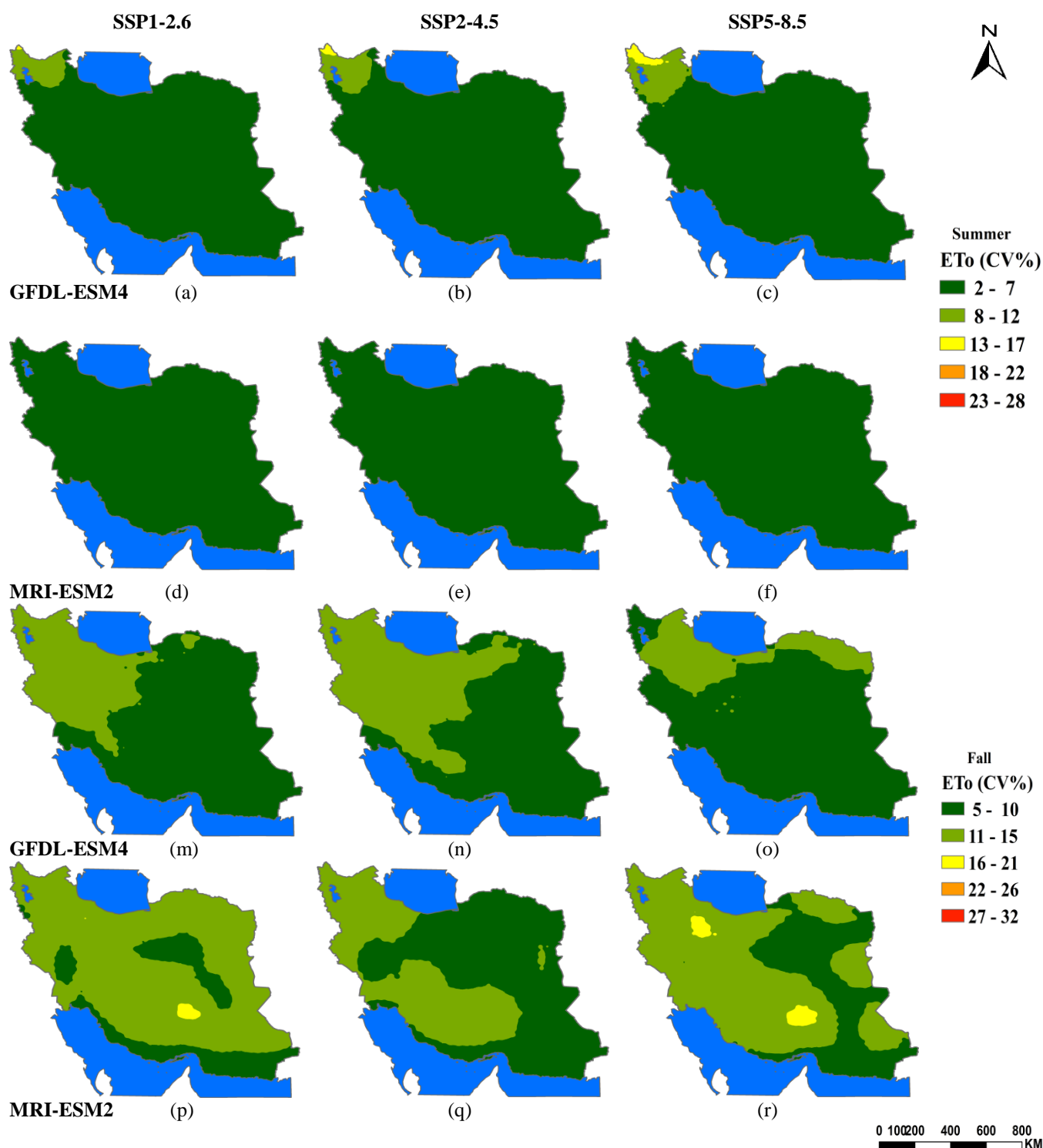


Figure 8. Average seasonal ETo changes in Summer (a to f) and Fall (m to r) under scenarios SSP1-2.6, SSP2-4.5 and SSP5-8.5 for 2020–2050.

4. Conclusion

The average ETo and its spatial changes in the past and future were examined in this study using station data and CMIP6 models. The output maps show that higher altitudes and latitudes significantly reduce ETo in Iran. Higher ETo values are seen in the

southwest, southeast and south of the country toward the interior regions throughout the year, except for summer in the observational period and the GFDL-ESM4 model scenarios in the future period (in which some areas of the southeast, especially the coastal areas affected by the monsoon system, have a

decrease in ET_0).

According to GFDL-ESM4, only under SSP5-8.5 in the winter would the areas in the southeast of Iran with more ET_0 expand. However in all scenarios of this model, ET_0 will decline throughout the year in Iran's northern half (particularly in the northwest and to some extent in the west and northeast). It will also decrease in the southeast and southwest of the country (except for winter in SSP5-8.5 conditions).

On the other hand, according to all three MRI-ESM2 model scenarios, the amount of ET_0 will rise in the southeast, south and interior parts of the country between 2020 and 2050, compared to the observational period. Regarding the regions with lower ET_0 , according to MRI-ESM2, the amount of ET_0 will decrease according to all three scenarios (in the northwest, west and east, as well as regions in Zagros throughout the winter). However in spring and summer, in addition to the increase of ET_0 in the Caspian coastal strip, it will also increase in the northeast, east of the Caspian Sea, west and interior areas in these seasons, and even in the northwest in summer. The biggest increases in ET_0 will happen under SSP5-8.5, SSP1-2.6 and SSP2-4.5 scenarios, respectively. Despite the fact that the regions in this study were categorized in low, medium and high evapotranspiration classes, it can be concluded in general that these regions have high evapotranspiration because of the lack of precipitation.

In terms of extent changes, most changes occurred during the observational period in the fall (in the southeastern areas of the Caspian Sea and around Kerman), summer (around Kerman), winter (the aforementioned areas of the fall and the northeast, northwest, and to some extent west Iran), and spring (around Kerman).

According to MRI-ESM2, the northeastern and eastern parts of the country as well as western regions of its inner plateau will encounter the greatest changes between 2020 and 2050 during the winter (21%–25%) under SSP1-2.6. Although, based on the other two scenarios of this model changes will increase in most regions of Iran (except for the northwest of the country and the southeast of the Caspian Sea under SSP2-4.5). A decline in changes is projected for other seasons of the year in different regions

of Iran based on the model scenarios compared to the observational period. Generally, GFDL-ESM4 shows that the amount of ET_0 changes is less than MRI-ESM2.

References

- Ajjur, S. B., & Al-Ghamdi, S. G. (2021). Evapotranspiration and water availability response to climate change in the Middle East and North Africa, *Climatic Change*, 166(3), 1-18. <https://doi.org/10.1007/s10584-021-03122-z>.
- Al-Hasani, A. A, J., & Shahid, S. (2022). Spatial Distribution of the Trends in Potential Evapotranspiration and its Influencing Climatic Factors in Iraq, *Theoretical and Applied Climatology*, 150, 677–696. <https://doi.org/10.1007/s00704-022-04184-4>.
- Alizadeh, A., & Salehnia, N. (2014). Application of Aridity Index in Determination of Potential Evapotranspiration for Estimating Crop Water Use in Iran, *Iranian Journal of Irrigation and Drainage*, 8(1), 136-144. https://idj.iaid.ir/article_54612.html?lang=en.
- Allen, R. G., Pereira, L. S., Raes, D., & Smith, M. (1998). FAO Irrigation and drainage paper No. 56, *Rome: Food and Agriculture Organization of the United Nations*, 56(97), e156.
- Allen, R. G., Smith, M., Perrier, A., & Pereira, L. S. (1994). An update for the definition of reference evapotranspiration, *ICID bulletin*, 43(2), 1-34.
- Amare, S., Langendoen, E., Keesstra, S., Ploeg, M. V. D., Gelagay, H., Lemma, H., & Zee, S. E. V. D. (2021). Susceptibility to gully erosion: Applying random forest (RF) and frequency ratio (FR) approaches to a small catchment in Ethiopia. *Water*, 13(2), 216. <https://doi.org/10.3390/w13020216>.
- Asadi, M., & Karami, M. (2020). Estimation of evapotranspiration in Fars province using experimental indicators, *Iranian Journal of Applied Researches in Geographical Sciences*, 20(56), 159-175. <https://www.sid.ir/paper/379096/en>.
- Bakhtiari, B., Khanjani, M. J., & Fadaei-Kermani, E. (2017). Differentiation of

- computed sum of hourly and daily reference evapotranspiration in a semi-arid climate, *Journal of Applied Research in Water and Wastewater*, 4(2), 358-362.
- Begueria, S., Vicente-Serrano, S. M., & Begueria, M. S. (2017). Package 'spei'. Calculation of the Standardised Precipitation-Evapotranspiration Index. <https://cran.r-project.org/web/packages/SPEI/index.html>.
- Chang, W., Cheng, J., Allaire, J., Xie, Y., & McPherson, J. (2017). Shiny: Web Application Framework for R. <https://CRAN.R-project.org/package=shiny>. Version 1.0.3
- Cheshmberah, F., & Zolfaghari, A. A. (2019). The effect of climate change on future reference evapotranspiration in different climatic zones of Iran, *Pure and Applied Geophysics*, 176(8), 3649-3664. <https://doi.org/10.1007/s00024-019-02148-w>.
- Dong, Q., Wang, W., Shao, Q., Xing, W., Ding, Y., & Fu, J. (2020). The response of reference evapotranspiration to climate change in Xinjiang, China: Historical changes, driving forces, and future projections, *International Journal of Climatology*, 40(1), 235-254. <https://doi.org/10.1002/joc.6206>.
- Eslami, A., & Ghahraman, B. (2013). Sensitivity analysis and uncertainty parameters affecting in the estimation of reference evapotranspiration in models with different mathematical structure. Iranian, *Journal of Irrigation and Drainage*, 7(1), 68-79. <https://www.sid.ir/paper/131644/en>.
- Eyring, V., Bony, S., Meehl, G. A., Senior, C. A., Stevens, B., Stouffer, R. J., & Taylor, K. E. (2016). Overview of the Coupled Model Intercomparison Project Phase 6 (CMIP6) experimental design and organization, *Geoscientific Model Development*, 9(5), 1937-1958. <https://doi.org/10.5194/gmd-9-1937-2016>.
- Gudarzi, M., Hosseini, S. A., & Mohammadi, N. (2018). Estimate of Potential Evapotranspiration in Kavir, Desert and Makren coast, *The 13th National Conference on Watershed Management Science & Engineering of Iran and the 3rd National Conference on Conservation of Natural Resources and Environment*, <https://civilica.com/doc/827329>.
- Heydari, M. M., Tajamoli, A., Ghoreishi, S. H., Darbe-Esfahani, M. K., & Gilasi, H. (2015). Evaluation and calibration of Blaney-Criddle equation for estimating reference evapotranspiration in semiarid and arid regions, *Environmental Earth Sciences*, 74, 4053-4063. <https://doi.org/10.1007/s12665-014-3809-1>.
- Heydari., T. K. S., & Khoshkhou, Y. (2019). Projection and prediction of the annual and seasonal future reference evapotranspiration time scales in the West of Iran under RCP emission scenarios, *Iranian Journal of Applied Researches in Geographical Sciences*, 19(53), 157-176. <https://doi.org/10.29252/jgs.19.53.157>.
- Hijmans, R. J., Van-Etten J., Cheng, J., Mattiuzzi, M., Sumner, M., & Greenberg, J. A. (2015). Package 'raster', *R package*, 1:734.
- IPCC (2013). Climate Change 2013: The Physical Science Basis. Contribution of Working Group I to the Fifth Assessment Report of the Intergovernmental Panel on Climate Change [Stocker T F D, Qin G K et al. (eds.)]. *Cambridge University Press, Cambridge, United Kingdom and New York, NY, USA*, 1535 pp. <https://doi.org/10.1017/CBO978110741532>.
- Kadkhodazadeh, M., Valikhan, A. M., Morshed, B. A., & Farzin, S. (2022). A new methodology for reference evapotranspiration prediction and uncertainty analysis under climate change conditions based on machine learning. multi criteria decision making and Monte Carlo methods, *Sustainability*, 14(5), 2601. <https://doi.org/10.3390/su14052601>.
- Kermani., E. F., Abbas-Barani, G., & Javad, Khanjani, M. (2014). Developing a framework for compatibility analysis of predictive climatic variables distribution with reference evapotranspiration in probabilistic analysis of water requirement, *Journal of Applied Research in Water and Wastewater*, 1(2), 66-73.
- Keshavarz, A., Malkian, R., Najhandali, A., & Beigi, A. (2021). The collection of documents related to the national and strategic document of food security evolution; Explanation of the country's

- water situation (No. 8). *Iran: Publication of Agricultural Education*.
- Khanmohammadi, N., Rezaie, H., Montaseri, M., & Behmanesh, J. (2017). The effect of different meteorological parameters on the temporal variations of reference evapotranspiration, *Environmental Earth Sciences*, 76, 1-13. <https://doi.org/10.1007/s12665-017-6871-7>.
- Lashkari, H., & Mohammadi, Z. (2019). Study on the role of annual movements of Arabian subtropical high pressure in the late start of precipitation in southern and southwestern Iran, *Theoretical and Applied Climatology*, 137(3), 2069-2076. <https://doi.org/10.1007/s00704-018-2716-x>.
- Li, Y., Liang, K., Bai, P., Feng, A., Liu, L., & Dong, G. (2016). The spatiotemporal variation of reference evapotranspiration and the contribution of its climatic factors in the Loess Plateau, China. *Environmental Earth Sciences*, 75, 1-14. <https://doi.org/10.1007/s12665-015-5208-7>.
- Li, Y., Yu, W., Wang, K., & Ma, X. (2019). Comparison of the aridity index and its drivers in eight climatic regions in China in recent years and in future projections, *International Journal of Climatology*, 39(14), 5256-5272. <https://doi.org/10.1002/joc.6137>.
- Liu, X., LI, C., Zhao, T., & Han, L. (2020). Future changes of global potential evapotranspiration simulated from CMIP5 to CMIP6 models, *Atmospheric and Oceanic Science Letters*, 13(6), 568-575. <https://doi.org/10.1080/16742834.2020.1824983>.
- Maghsoudi, M. (2020). Desert landscapes and landforms of Iran, *Springer Nature*.
- Majumder, M. (2015). Impact of urbanization on water shortage in face of climatic aberrations, *Springer*.
- Masoompour, S. J., Rajaei, S., & Yeganehfar, M. (2014). Temporal-spatial variability and evapotranspiration trend of the reference plant in Iran, *Iranian Journal of Applied Researches in Geographical Sciences*, 14(34), 7-25. <https://jgs.khu.ac.ir/article-1-2067-fa.html>.
- Miri, M., Masoompour, S. J., Raziei, T., Jalilian, A., & Mahmodi, M. (2021). Spatial and temporal variability of temperature in Iran for the twenty-first century foreseen by the CMIP5 GCM models, *Pure and Applied Geophysics*, 178(1), 169-184. <https://doi.org/10.1007/s00024-020-02631-9>.
- Modaresi, F., & Araghi, A. (2023). Projecting future reference evapotranspiration in Iran based on CMIP6 multi-model ensemble, *Theoretical and Applied Climatology*, <https://doi.org/10.1007/s00704-023-04465-6>.
- Mokhtar, A., He, H., Alsafadi, K., Li, Y., Zhao, H., Keo, S., Bai, CH., Abuarab, M., Zhag, Ch., Elbaagoury, K., Wang, J., & He, Q. (2020). Evapotranspiration as a response to climate variability and ecosystem changes in southwest, China, *Environmental Earth Sciences*, 79, 1-21. <https://doi.org/10.1007/s12665-020-09007-1>.
- Mulla, D. J., & Mc-Bratney, A. B. (2001). Soil spatial variability. Soil physics companion, *CRC Press, Boca Raton*, 343-373.
- Newton, I. H., Islam, G. T., Islam, A. S., Razzaque, S., & Bala, S. K. (2021). A conjugate application of MODIS/Terra data and empirical method to assess reference evapotranspiration for the southwest region of Bangladesh, *Environmental Earth Sciences*, 80(6), 223. <https://doi.org/10.1007/s12665-021-09482-0>.
- Nouri, M., Homaei, M., & Bannayan, M. (2017). An Assessment of reference evapotranspiration changes during the 21st century in some semi-arid regions of Iran, *Iranian Journal of Soil and Water Research*, 48(2), 241-252. <https://doi.org/10.22059/ijswr.2017.62578>.
- Obada, E., Alamou, E. A., Chabi, A., Zandagba, J., & Afouda, A. (2017). Trends and changes in recent and future Penman-Monteith potential evapotranspiration in Benin (West Africa), *Hydrology*, 4(3), 38. <https://doi.org/10.3390/hydrology4030038>.
- Oki, T., & Kanae, S. (2006). Global hydrological cycles and world water resources, *Science*, 313 (5790), 1068-

1072.
<https://doi.org/10.1126/science.1128845>.
- Pan, S., Pan, N., Tian, H., Friedlingstein, P., Sitch, S., Shi, H., Arora, V. K., Haverd, V., Jain, A. K., Kato, E., Lienert, S., Lombardozzi, D., Nabel, J. E. M. S., Otle, C., Poulter, B., Zaehle, S., & Running, S. W. (2020). Evaluation of global terrestrial evapotranspiration using state-of-the-art approaches in remote sensing, machine learning and land surface modeling, *Hydrology and earth system sciences*, 24(3), 1485-1509. <https://doi.org/10.5194/hess-24-1485-2020>.
- Parding, K. M., Dobler, A., McSweeney, C. F., Landgren, O. A., Benestad, R., Erlandsen, H. B., Mezghani, A., Gregow, H., Rati, O., Viktor, E., El Zohbi, J., Christensen, O. B., & Loukos, H. (2020). GCMeval—An interactive tool for evaluation and selection of climate model ensembles, *Climate Services*, 18, 100167. <https://doi.org/10.1016/j.cliser.2020.100167>.
- Pour, S. H., Abd-Wahab, A. K., Shahid, S., & Ismail, Z. B. (2020a). Changes in reference evapotranspiration and its driving factors in peninsular Malaysia, *Atmospheric Research*, 246, 105096. <https://doi.org/10.1016/j.atmosres.2020.105096>.
- Pour, S. H., Abd-Wahab, A. K., & Shahid, S. (2020b). Spatiotemporal changes in aridity and the shift of drylands in Iran, *Atmospheric Research*, 233, 104704. <https://doi.org/10.1016/j.atmosres.2019.104704>.
- Qi, P., Zhang, G., Xu, Y. J., Wu, Y., & Gao, Z. (2017). Spatiotemporal changes of reference evapotranspiration in the highest-latitude region of China, *Water*, 9(7), 493. <https://doi.org/10.3390/w9070493>.
- Rahimi, M. (2012). Analyzing the temporal and spatial variation of fog days in Iran, *Pure and applied geophysics*, 169(5), 1165-1172. <https://doi.org/10.1007/s00024-011-0326-y>.
- Raziei, T., & Porehkar, A. (2021). Performance evaluation of NCEP/NCAR reanalysis blended with observation-based datasets for estimating reference evapotranspiration across Iran, *Theoretical and Applied Climatology*, 144(3), 885-903. <https://doi.org/10.1007/s00704-021-03578-0>.
- Riahi, K., Van Vuuren, D. P., Kriegler, E., Edmonds, J., O'neill, B. C., Fujimori, S., Bauer, N., Calvin, K., Dellink, R., Fricko, O., Lutz, W., Popp, A., Cuaresma, J. C., KC, S., Leimbach, M., Jiang, L., Kram, T., Rao, Sh., Emmerling, J., Ebi, K., Hasegawa, T., Havlik, P., Humpenoder, F., Da Silva, L. A., Smith, S., Stehfest, E., Bosetti, V., Eom, J., Gernaat, D., Masui, T., Rogelj, J., Sterefer, J., Drouet, F., Krey, V., Luderer, G., Harmsen, m., Takahashi, A., Baumstark, L., Doelman, J. C., Kainuma, M., Klimont, Z., Marangoni, G., Lotze-Campen, H., Oberteiner, M., Tabeau, A., & Tavoni, M. (2017). The shared socioeconomic pathways and their energy, land use, and greenhouse gas emissions implications: an overview, *Global Environmental Change* 42, 153-168. <https://doi.org/10.1016/j.gloenvcha.2016.05.009>.
- Shah, S. A. (2022). Hargreaves-Samani method: Estimation of historical annual, seasonal, and monthly Reference Evapotranspiration (ET_o) in Dadu District, Pakistan, *Journal of Applied Research in Water and Wastewater*, 9(1), 30-39.
- Sharafi, S., & Mohammadi-Ghaleni, M. (2021). Calibration of empirical equations for estimating reference evapotranspiration in different climates of Iran, *Theoretical and Applied Climatology* 145(3), 925-939. <https://doi.org/10.1007/s00704-021-03654-5>.
- Shirmohammadi, Z., Kouhi, M., Mohammadian, A., Habibi-Nokhandan, M., Mirzaee, M. J., & Mododi, M. N. (2018). Spatial and temporal characteristics of Reference evapotranspiration using CRU gridded datasets and prediction of its changes during future periods in Khorasan Razavi, *Iranian Journal of Climate Research*, 9(33), 89-109. https://clima.irimo.ir/article_77189.html?lang=en.
- Soltani, M., Laux, P., Kunstmann, H., Stan, K., Sohrabi, M. M., Molanejad, M.,

- Sabzipavar, A. A., Ranjbar Saadatabadi, A., Ranjbar, F., Rousta, I., Zawar-Reza, P., Khoshakhlagh, F., Soltanzadeh, I., Babu, C. A., Azizi, G. H., & Martin, M. V. (2016). Assessment of climate variations in temperature and precipitation extreme events over Iran, *Theoretical and Applied Climatology*, 126(3-4), 775-795. <https://doi.org/10.1007/s00704-015-1609-5>.
- Tabari, H., Marofi, S., Aeini, A., Talaei, P. H., & Mohammadi, K. (2011). Trend analysis of reference evapotranspiration in the western half of Iran, *Agricultural and forest meteorology*, 151(2), 128-136. <https://doi.org/10.1016/j.agrformet.2010.09.009>.
- Tabari, H., & Talaei, P. H. (2011). Analysis of trends in temperature data in arid and semi-arid regions of Iran, *Global and Planetary Change*, 79(1-2), 1-10. <https://doi.org/10.1016/j.gloplacha.2011.07.008>.
- Wang, Z., Zhan, C., Ning, L., & Guo, H. (2021). Evaluation of global terrestrial evapotranspiration in CMIP6 models, *Theoretical and Applied Climatology*, 143(1), 521-531. <https://doi.org/10.1007/s00704-020-03437-4>.
- Zarrin, A., & Salehabadi, N. (2019). Drought projection in Tehran based on CMIP6 models, *6th international-regional conference on climate change. Iran. Tehran*, <https://civilica.com/doc/1002617/>.
- Zhao, J., Xia, H., Yue, Q., & Wang, Z. (2020). Spatiotemporal variation in reference evapotranspiration and its contributing climatic factors in China under future scenarios, *International Journal of Climatology*, 40(8), 3813-3831. <https://doi.org/10.1002/joc.6429>.